Journal of Applied Research in Water and Wastewater
E-ISSN: 2476-6283
Journal homepage: https://arww.razi.ac.ir

Optimization of the $Fe_3O_4/Fe_xCu_yW_zO_t$ photocatalyst for 2,4 dichlorophenoxyacetic acid wastewater degradation using the response surface method

Saeed Khanlari, Faranak Akhlaghian*

Department of Chemical Engineering, Faculty of Engineering, University of Kurdistan, Sanandaj, Iran.

GRAPHICAL ABSTRACT

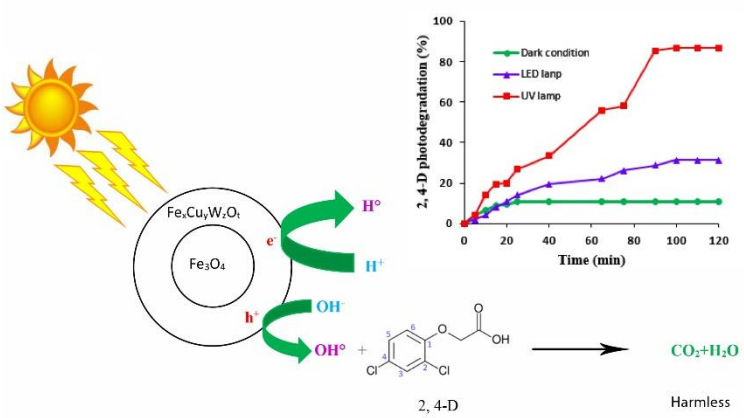

ARTICLE INFO

Article history:
Received 1 September 2021
Reviewed 5 November 2021
Received in revised form 20 December 2021
Accepted 23 December 2021
Available online 26 December 2021

Keywords:
Core/shell
2, 4-D wastewater
Magnetite
WO_3

Article type: Research Article

ABSTRACT

Herbicides such as 2, 4-dichlorophenoxyacetic acid (2, 4-D) are generally carcinogenic and their existence in water cause many problems. In this work, $Fe_3O_4/Fe_xCu_yW_zO_t$ core/shell magnetic photocatalyst was used to remove 2, 4-D. The statistical analysis of the results of the Box-Behnken experimental design method revealed that among the constituents of the photocatalyst shell, iron had the highest effect on 2, 4-D photodegradation. The photocatalyst composition was optimized using the response surface method. The photocatalyst formulation was determined using ICP method: $Fe_3O_4/Fe0.874Cu0.349W0.004O1.525$. XRD analysis confirmed the formation of Fe_3O_4, CuO, and WO_3 in the photocatalyst shell. TEM images showed the photocatalyst core/shell structure. $Fe_3O_4/Fe0.874Cu0.349W0.004O1.525$ photodegraded 2, 4-D under ultraviolet light irradiation with the maximum yield of 90%. The photocatalyst was also active under sunlight and LED. The kinetics of the 2, 4-D photodegradation reaction under ultra violet light irradiation was studied. It followed first order kinetic model. The rate constant of the reaction was 0.0118 min^{-1}. The photocatalyst activity of $Fe_3O_4/Fe_{0.874}Cu_{0.349}W_{0.004}O_{1.525}$ remained constant after the fourth cycle of reuse, which is the good advantage.

1. Introduction

Large amounts of herbicides are used in agriculture, and their excess amount remains in water and soil causing water sources to be polluted. Herbicides are toxic, carcinogenic, and neurotoxic; and also can interfere in the cell division process (Seck et al. 2012; Marin-Morales et al. 2013; Yusa et al. 2015). Thus, it is necessary to develop an efficient technology to remove herbicides from water. 2, 4-dichlorophenoxyacetic acid, or shortly 2, 4-D is the most common herbicide in the world (Browne & Moore 2014; Costa & Aschner 2014). The 2, 4-D compound is used in the mixture of utilized herbicides to destroy broadleaf weeds (Youssef et al. 2017). Exposure to 2, 4-D can cause blood, liver and kidney poisoning; skin and eye irritation; and cancer (Tang et al. 2012; Tang et al. 2015; Youssef et al. 2017). The environmental protection agency limited the allowable concentration of 2, 4-D in water to 0.1 mg/L. The World Health Organization determined the maximum level of 2, 4-D in water 70 µg/L (National drinking water regulations: 2,4-D, 1995; Kunda 2005). Many processes have been suggested to remove 2, 4-D from water including absorption, adsorption, biological treatment, and advanced oxidation processes.

However; some of these methods need secondary treatment units, are inefficient in low concentration, or expensive (Dnaeshvar et al. 2004; Wu et al. 2007; Gherbi et al. 2011; Dong et al. 2015; Pham et al. 2016). Photocatalysis is one of the advanced oxidation processes for

*Corresponding author Email: akhlaghianfk@gmail.com

How to cite: S. Khanlari, F. Akhlaghian, Optimization of the Fe_3O_4/FexCuyWzOt photocatalyst for 2,4 dichlorophenoxyacetic acid wastewater degradation using the response surface method, *Journal of Applied Research in Water and Wastewater*, 8 (2), 20121, 160-168.

removing pollutants from water. Photocatalysis has advantages like pollutants oxidation and conversion them to harmless inorganic compounds (H_2O and CO_2), no secondary pollution, remove pollutants in low concentrations, available cheap active photocatalysts, ability to apply for a wide range of organic compounds, operation in the temperature and pressure of room (Rebelo et al. 2007; Chang et al. 2015; Hatamzadeh et al. 2019; Nasir et al. 2020; Rabanimehr et al. 2021). Photocatalysts used semiconductors which generate electron-hole pairs at their surface under ultraviolet-visible light irradiation. The generated holes can react with water molecules and hydroxyl ions and strong oxidants like hydroxyl radicals are generated, which attack organic compounds and convert them to minerals (H_2O and CO_2) (Abdollahi et al. 2011; Widiyandari 2012; Momeni 2015). The photocatalytic degradation of 2, 4-D was investigated by several researchers. Lam et al. (2013) loaded MoO_3 on ZnO nanorods and applied it for 2, 4-D photodegradation. Macía-Tamez et al. (2016) used WO_3/TiO_2, Fe_2O_3/TiO_2, and TiO_2 catalysts in 2, 4-D photodegradation, and their results showed that doping with WO_3 and Fe_2O_3 improved TiO_2 photocatalytic activity. Huy et al. (2017) showed stable photocatalytic activity of $TiO_2@MgFe_2O_4$ for 2,4 –D removal after four cycles of reuse. Chenchana et al. (2019) synthesized the TiO_2 nanobelt enriched with anatase phase and deposited Au on it. They obtained the yield of 99.2% for 2, 4-D removal. Fiorenza et al. (2019) imprinted TiO_2 with 2, 4-D and applied it for 2, 4-D photodegradation. They reported the removal yield of 74%. Gu et al. (2018) synthesized the Co_9S_8/graphite carbon nitride photocatalyst using the hydrothermal method, and found that Cr(VI) reduction and 2, 4-D oxidation were higher when the both pollutants existed. Mehrabadi and Faghihian (2019) immobilized TiO_2 on clinoptilolite surface, and reported that the TiO_2 deposition on clinoptilolite improved the photocatalytic activity for 2, 4-D degradation. Most of these photocatalysts have the problem of difficult separation from water.

Magnetic photocatalysts with the advantage of easy separation from water usually possess core/shell structure (Aghel et al. 2016; Ding et al. 2016; Arsalani et al. 2019). Core/shell structure has the advantages of stable magnetic core and prevention of core leaching, and enjoying the properties of core and shell together (Kalambate et al. 2019; Xie et al. 2019; Banihashemi et al. 2020). Moreover, it was shown that CuO and WO_3 were good photocatalysts for the photodegradation of organic pollutants from water (Akhlaghian & Najafi 2018; Habibi-Yangjeh & Mousavi 2018). Accordingly, in this work, the magnetic photocatalyst $Fe_3O_4/Fe_xCu_yW_zO_t$ was used to remove 2, 4-D from water. The compositions of Cu, W, and Fe was optimized using the response surface method. The effect of Fe_3O_4 was also investigated. The optimized photocatalyst $Fe_3O_4/Fe_xCu_yW_zO_t$ was characterized using the ICP, ASAP, XRD, SEM, and TEM techniques. The kinetics of the reaction, effects of light sources, and stability were also investigated.

2. Materials and methods

2.1. Materials

Acetone, iron (II) sulfate heptahydrate, iron (III) chloride anhydrous, sodium tungstate dihydrate, copper (II) nitrate trihydrate, sodium citrate dihydrate, hydrazine hydrate (80% aqueous solution), ammonia (25% aqueous solution), sodium hydroxide all were purchased from Merck Company (Germany). 2, 4-Dichlorophenoxyacetic acid (97%) was from Sigma-Aldrich.

2.2. Photocatalyst preparation

The solutions of Fe^{3+} and Fe^{2+} with the concentrations of 0.5 molar at the Fe^{+3}: Fe^{2+} volumetric ratio of 1:1.75 were mixed. The mixture was stirred at 60°C under protection of nitrogen gas for 10 min in the three mouth flask. Then, 5 mL of hydrazine and 10 mL of ammonia were added (Hong et al. 2009). The pH of the solution was maintained at 9 by dropwise addition of ammonia for 30 min. After reaction, the black precipitate was separated by an external magnet. The precipitate was washed with deionized water for several times until the pH of the wash water reached 7. The precipitate Fe_3O_4 was dried at 70°C for 12 h (Hong et al. 2008; Hong et al. 2009). One gram of dried Fe_3O_4 was distributed ultrasonically in 200 mL of sodium citrate solution with the concentration of 0.87 molar for 30 min. The mixture was mixed by magnetic stirrer at 60°C under protection of N_2 gas for 12 h. The resultant precipitate was separated magnetically, washed with acetone to remove the remainder of citrate ions. At this stage, the Fe_3O_4 modified by citrate was produced (Hong et al. 2008; Hong et al. 2009).

The final stage of catalyst preparation was coating by shell. Fifty mL of Fe^{3+} (x molar), Cu^{2+} (y molar), and sodium tungstate (z molar) were mixed at 90°C under protection of nitrogen gas for 10 min in the three mouth flask. The x, y, and z were determined according to the design of experiments (Table 1). One gram of modified Fe_3O_4 was added to the solution and were stirred at 90°C for 30 min. Afterwards, 100 mL of sodium hydroxide solution was added to the mixture and stirred for 2 h. The produced precipitate was separated magnetically from the solution, washed with deionized water until wash water with pH 7 was obtained (Hong et al. 2008; Hong et al. 2009; Mirzapour and Akhlaghian. 2019).

2.3. Characterization instruments

The inductively coupled plasma atomic emission spectrometer, Varian ICP-OES 730-ES was used to determine the iron, copper, and tungsten compositions of the shell and core/shell samples. The XRD patterns of the magnetite, modified magnetite, shell, and core/shell samples were obtained to investigate and compare the crystalline structure of them. The XRD analyses were obtained by radiating Co k_α (λ=1.489 Å) at 40 kV and 40 mA, in the 2θ range of 0 to 90° with the scan rate of 2°/s with the XRD equipment PW 1730 from Phillips Company. Scanning electron microscope TESCAN-MIRA3 was used to investigate the surface morphology and crystalline structure of the samples. Philips transmission electron microscope was used to recognize the core/shell structure of the photocatalyst. The N_2 adsorption/desorption isotherm which was obtained by Micrometrics ASAP 2020 equipment to determine the porosimetry and specific surface area of the samples. The magnetometer from Kavir Company was used to investigate the magnetic properties of the samples.

2.4. Photocatalytic experiments

The batch experiment of 2,4-D removal was done by addition 0.1 g of the prepared core/shell photocatalyst to the 100 mL of the 2, 4-D solution with the concentration of 10 mg/L in a 2 L beaker which was placed on a magnetic stirrer at room temperature for 2 h under ultra violet (UV) light irradiation. The schematic of the used set-up was shown in our previous work (Mirazi et al. 2019). After the time of reaction, the core/shell photocatalyst was separated magnetically. The UV-Vis spectrometer (T80+ from PG Instruments) was used to determine the concentration of 2, 4-D in the solution at the wavelength of 284 nm. The yield of 2, 4-D removal was determined using the following equation (Atarodi and Faghihian. 2019):

$$\text{D removal}\ (\%) = \frac{A_0 - A}{A_0} \times 100 \quad (1)$$

A_0 and A were the absorption of the initial solution and sample, respectively. Each experiment was repeated at least three times.

2.5. Design of experiments

Among the response surface methods, Box-Behnken method was used to optimize the $Fe_3O_4/Fe_xCu_yW_zO_t$ formulation. The effects of the independent variables, concentrations of Fe(III), tungstate, and Cu(II) solutions were investigated on 2,4 dichlorophenoxyacetic acid (2, 4-D) photodegradation. Table 1 shows the design of experiments using Box-Behnken method and Design Expert software (Version 11).

3. Results and discussion

3.1. Experimental modeling

Table 2 shows the results of analysis of variance. The high F-value (2869.37) and low p-value (<0.0001) show the significance of the model in 99.9% confidence level. The signal to noise ratio is reported 227.869 which is favorable. The quadratic equation suggested by design expert software (Version 11) to predict the 2, 4-D removal (Eq. 2) is:

$$\text{D removal}\ (\%) = 13.9585 + 12.918A - 14.0515B + 45.0185C - 1.575AB - 6.305AC - 9.3BC + 0.866A^2 + 39.214B^2 - 29.586C^2 \quad (2)$$

where, A, B, and C are Fe^{3+}, Cu^{2+}, and tungstate solutions concentrations (mol/L), respectively. Fig. 1 shows good correspondence between experimental and predicted results. Correlation coefficient R^2 (0.9997) and adj R^2 (0.9994) confirmed this agreement. Standard deviation was 0.3. Table 2 indicates the significance of different terms of Eq. 2. Table 2 shows that the linear term of Fe(III) concentration (F-value 10094.1), linear term of Cu(II) concentration (F-value 788.4), and quadratic term of Cu(II)

concentration (F-value 2145.41) had the highest effects on the 2, 4-D photodegradation.

The effects of the tungsten concentration terms were lower due to their smaller F-value. The interaction terms of Fe-W (F-value 437.29) and Cu-W (F-value of 237.5) had also considerable effects on the response.

The contour plots of the response can help to better understand 2,4-D photocatalyst degradation process. As shown in Fig. 2a, in the constant values of Cu and W, an increase in Fe concentration improved 2,4-D photodegradation. This Fig. also shows that optimum amounts of Cu concentration depended on the Fe. Moreover, the optimum amounts of W concentration were related to the Cu, as shown in Fig. 2 a.

Table 1. Design of experiments, and experimental and predicted results.

No.	Fe^{+3} concentration, mol/L	Cu^{+2} concentration, mol/L	WO_4^{-2} concentration, mol/L	2, 4-D photodegradation, %	
				Experimental	Modeling
1	0	0.5	0	16.80	16.73
2	1	0.5	0.5	39.70	39.36
3	2	0.5	0	44.52	44.46
4	1	1	1	51.51	51.15
5	1	0	0	27.75	27.74
6	1	1	0	51.20	51.33
7	1	0	1	37.00	36.87
8	1	0.5	0.5	39.00	39.36
9	2	0	0.5	52.00	52.06
10	2	1	0.5	69.50	69.42
11	1	0.5	0.5	39.00	39.36
12	0	0	0.5	29.00	29.07
13	1	0.5	0.5	39.34	39.36
14	0	0.5	1	27.46	27.51
15	1	0.5	0.5	39.80	39.36
16	0	1	0.5	49.65	49.58
17	2	0.5	1	42.57	42.63

Table 2. Analysis of variance.

Source	F-value	p-value	
Model	2869.93	<0.0001	Significant
A-Fe^{+3} concentration (mol/L)	10094.10	<0.0001	
B-Cu^{+2} concentration (mol/L)	7889.94	<0.0001	
C-WO_4^{-2} Concertation (mol/L)	441.06	<0.0001	
AB	27.29	0.0012	
AC	437.29	<0.0001	
BC	237.85	<0.0001	
A^2	34.74	0.0006	
B^2	4451.41	<0.0001	
C^2	2533.89	<0.0001	
Residual			
Lack of Fit	0.1529	0.9185	Not significant

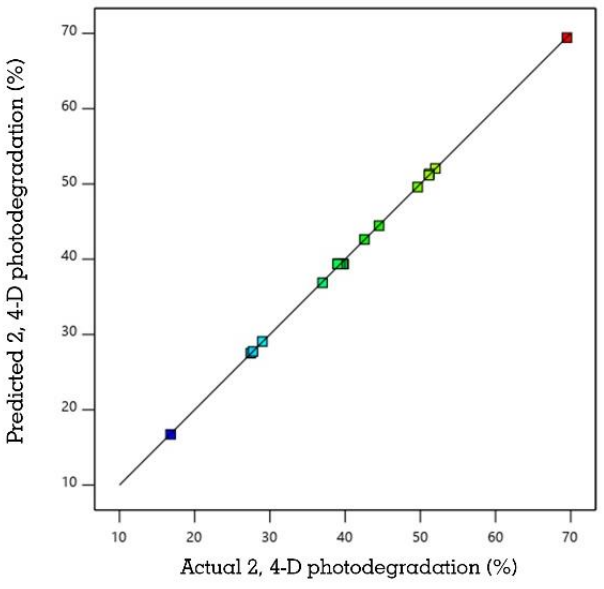

Fig. 1. Predicted versus actual response for 2,4-D photodegradation.

3.2. Photocatalyst optimization

Design expert software (Version 11) was used to determine the optimum of the variables which maximize 2,4 dichlorophenoxyacetic acid (2, 4-D) photodegradation. One of the optimum points suggested by the software was selected and tested experimentally for verification. The results are shown in Table 3. The difference between experimental and modeling results was less than 5 %.

3.2.1. Effect of core

In the experimental design tests, the Fe_3O_4 core amount was constant (1 g). In this section, the effect of Fe_3O_4 core on the 2,4-D photodegradation was investigated. It was shown in Fig. 3 that with increase in the Fe_3O_4, 2,4-D photodegradation first reached to a maximum and then decrease. The dipole-dipole attractive forces between core/shell magnetic nanoparticles of $Fe_3O_4/Fe_xCu_yW_zO_t$ increase particles aggregation. Therefore, increase in Fe_3O_4 core caused aggregation of nanoparticles, creation of larger particles, reduction of effective particles specific surface area, and decrease the yield of the photodegradation reaction (Hong et al. 2008). Therefore; in this work, the optimized photocatalyst was prepared by 1 g Fe_3O_4 and solution concentrations of the shell constituents: Fe^{3+} 1.99 mol/L, Cu^{2+} 0.99 mol/L, and WO^{4-} 0.38 mol/L. This optimized photocatalyst was used for characterization and investigation of the photocatalyst activity.

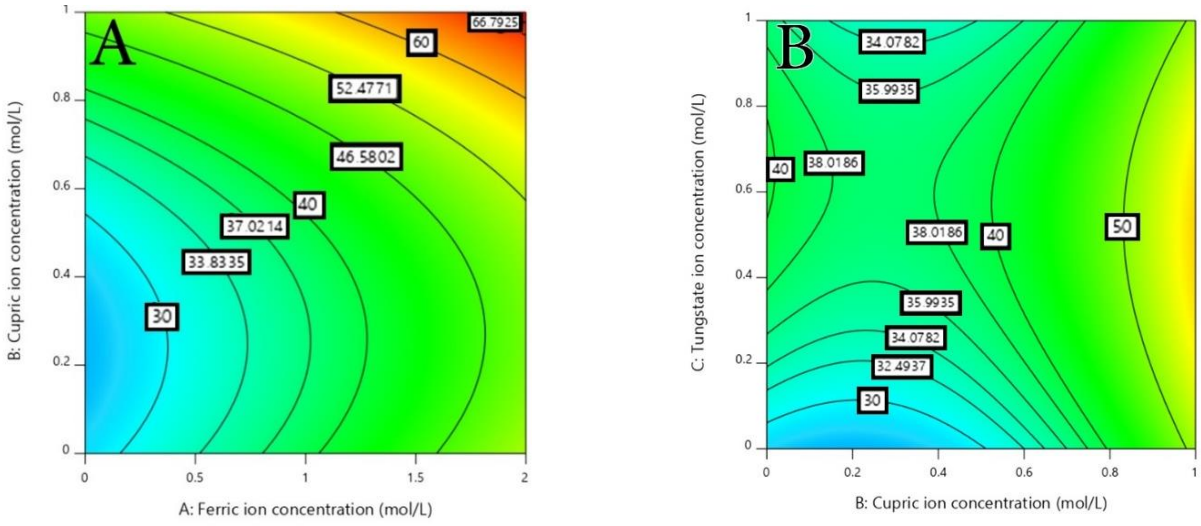

(a) (b)

Fig. 2. Contour plots of the 2, 4-D photodegradation, (a) WO_4^{2-} concentration was 0.459 mol/L; (b) Fe^{3+} concentration was 2 mol/L; operating conditions: 2,4-D initial concentration 50 mg/L, catalyst dose 1g/L, pH 6.5, time 120 min.

Table 3. Optimized parameters for photocatalyst preparation and response.

Fe^{+3} concentration, mol/L	Cu^{+2} concentration, mol/L	WO_4^{-2} concentration, mol/L	2, 4-D photodegradation, %	
			Experimental	Modeling
1.99	0.99	0.38	73.31	69.75

† operating conditions: 2,4-D initial concentration 50 mg/L, catalyst dose 1 g /L, pH 6.5, time 120 min

Table 4. Metal analysis of the shell and core/shell samples.

Sample	Type of element		
	Cu at λmax of 327.395 nm	Cu at λmax of 259.940 nm	W at λmax of 222.590 nm
Blank, wt. %	0.00	0.00	0.00
Shell, wt. %	23.03	50.85	0.76
Core/shell, wt. %	21.17	52.60	0.70

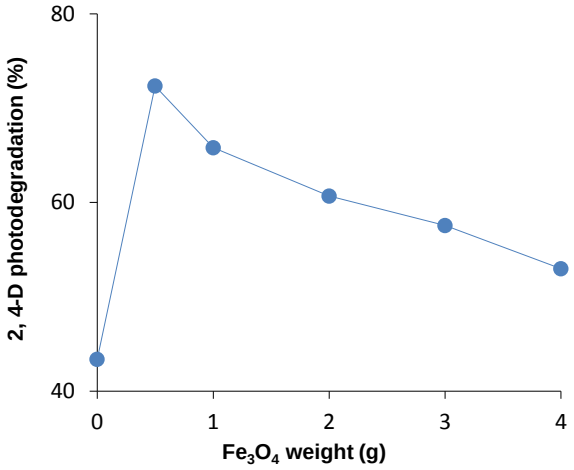

Fig. 3. Effect of Fe_3O_4 core on 2, 4-D photodegradation; operating conditions: 2,4-D initial concentration 50 mg/L, catalyst dose 1g /L, pH 6.5, time 120 min.

3.3. Photocatalyst characterization

Inductively coupled plasma was used to determine the composition of the shell and core/shell photocatalyst. The composition of the core/shell photocatalyst was: Fe_3O_4 core 3.52 % and in the shell Fe_3O_4 67.61%, CuO 27.78 %, and WO_3 1.018 % according to the results of Table 4. The optimized formula of the photocatalyst was determined to be $Fe_3O_4/Fe_{0.874}Cu_{0.349}W_{0.004}O_{1.525}$. XRD patterns of the core, modified core by citrate, shell, and core/shell nanoparticles are shown in Fig. 4. In the core and modified core samples, peaks at 21, 35, 41, 50, 63, 67, 74, and 85° were recognized which confirmed formation of magnetite with orthorhombic structure (JCPDS File No. 75-16109) (Chen et al. 2017). XRD patterns of the shell also shows peaks at 21.41, 35.18, 41.57, 50.58, 57.00, 63.28, 67.67 and 74.64° indicated the presence of Fe_3O_4 (JCPDS File No. 75-1609). Peaks at 41.57, 45.50, 57.00, 63.28, 67.67, 81.40, and 86.47° showed the existence of monoclinic CuO (JCPDS File No. 41-0254). Moreover, peaks at 45.50, 50.00, 63.28, 67.67, 74.64, 81.40, and 86.47° were related to the WO_3 with the monoclinic crystalline structure (JCPDS File No. 87-.2391) (Suresh et al. 2016; Mohite & Garg 2017; Wu et al. 2018).

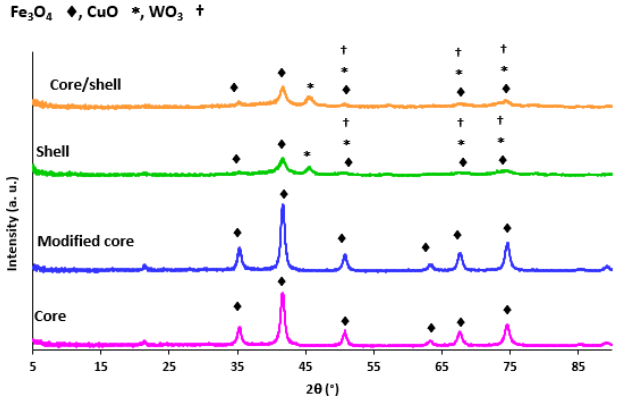

Fig. 4. XRD patterns of the core, modified core by citrate, shell, and core/shell samples.

In XRD pattern of the core/shell sample, Fe_3O_4 peaks were recognized at 21.42, 35.24, 41.62, 50.54, 57.08, 63.47, 67.50, 74.33, and 84.99° (JCPDS File No. 75-1609), CuO peaks were identified at 41.62, 45.54, 57.08, 80.08, 81.62, and 86.26° (JCPDS File No. 41-0256), and WO_3 peaks were at 45.54, 50.69, 63.47, 67.50, 68.67, 72.81, 74.33, 81.62, and 89.08° (JCPDS File No. 87-2391) (Suresh et al. 2016; Mohit & Garg 2017; Wu et al. 2018). The mean crystalline size of the nanoparticles was determined by Scherrer equation (Eq. 3):

$$D = \frac{k\lambda}{\beta\cos\theta} \quad (3)$$

where, D is the crystalline size of the nanoparticles in nm, k is a constant and equals 0.9, λ is the wavelength of the used cobalt tube, and here equals 17.890 nm, β is the diffraction peaks full width at half maximum (FWHM), and θ is the Bragg angle (Khairy. 2014). The crystalline size of the core, modified core, shell, and core/shell nanoparticles were 9.6, 4.84, 9.8, and 10.6 nm; respectively. The modified core had more

regular structure without aggregation which made the nanoparticles size smaller. The larger size of the core/shell nanoparticles confirmed coating of the core by shell and formation of the core/shell structure nanoparticles (Khairy. 2014).

SEM images of the core, shell, and core/shell nanoparticles are displayed in Fig. 5. The porous structure of the core, shell, and core/shell samples are completely clear. In the SEM images, the size of magnetic nanoparticles of core Fe_3O_4 were in the range of 15 to 31 nm, shell nanoparticles in the range of 29 to 75 nm, and core/shell nanoparticles $Fe_3O_4/Fe_{0.874}Cu_{0.349}W_{0.004}O_{1.525}$ were in the range of 7 to 82 nm. TEM images of the magnetic core/shell nanoparticles are shown in Fig. 6. The core/shell structure of the sample is clear. The darker points are Fe_3O_4 core and brighter parts belonged to the shell $Fe_{0.874}Cu_{0.349}W_{0.004}O_{1.525}$ due to their different electron diffusivities, their colors were different. Magnetic nanoparticles were aggregated due to dipole attractive interaction (Hong et al. 2009).

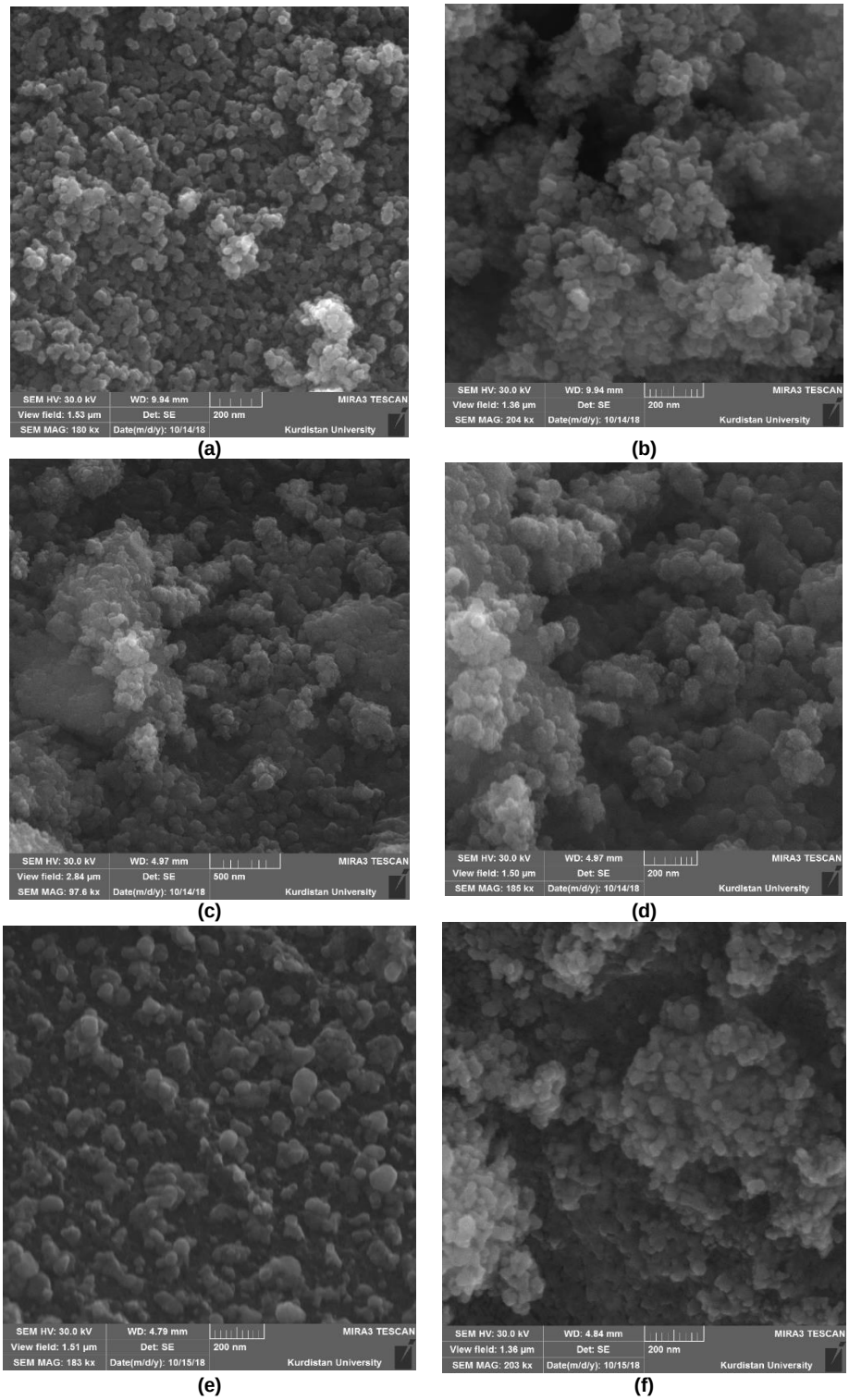

Fig. 5. SEM images of (A), (B) core; (C), (D) shell; and (E), (F) core/shell nanoparticles.

Fig. 7 a shows nitrogen adsorption/desorption isotherms for magnetic core/shell nanoparticles of $Fe_3O_4/Fe_{0.874}Cu_{0.349}W_{0.004}O_{1.525}$. The photocatalyst was mesoporous type IV, and its hysteresis was H3. It means the photocatalyst was formed from aggregation of particles with slit shape pores (Leofanti et al. 1998). Pore volume distribution was multimodal with peaks at 5.2 and 8.6 nm, as shown in Fig. 7 b. The pores with the diameter of 5.2 nm were the most prevalent. For pore larger than 8.6 nm, the pore prevalence decreases with the increase of diameter. The $Fe_3O_4/Fe_{0.874}Cu_{0.349}W_{0.004}O_{1.525}$ photocatalyst specific surface area, average pore diameter, and pore volume were 154.5 m^2/g, 5.25 nm, and 0.2028 m^3/g; respectively, according to the BJH desorption isotherm. The magnetic property of the synthesized nanoparticles was investigated by vibrating sample magnetometer analysis. According to Fig. 8 shows the $Fe_3O_4/Fe_{0.874}Cu_{0.349}W_{0.004}O_{1.525}$

nanoparticles are superparamagnetic. The saturation magnetism of core, shell, and core/shell samples were 66.05, 22.11, and 28.45 emu/g; respectively. The magnetic property of the shell decreased due to the dilution of its composition by CuO and WO_3. The magnetic property of the core/shell sample is smaller than Fe_3O_4 core. The existence of shell layer with smaller magnetic property in the core/shell sample caused reduction in saturated magnetism. Fig. 9 shows the effect of pH on 2,4 dichlorophenoxyacetic acid (2, 4-D) photodegradation. Dilute solutions of sodium hydroxide and hydrochloric acid were used to adjust the pH in the range of 2 to 10. The dissociation constant (pK_a) of 2,4 –D is 2.64. In acidic pH higher than 2.64, the $Fe_3O_4/Fe_{0.874}Cu_{0.349}W_{0.004}O_{1.525}$ photocatalyst surface was positive, and 2, 4-D molecules were charged negatively; so the attraction forces between 2, 4-D molecules and positive photocatalyst surface caused adsorption, and consequently photodegradation of 2, 4-D.

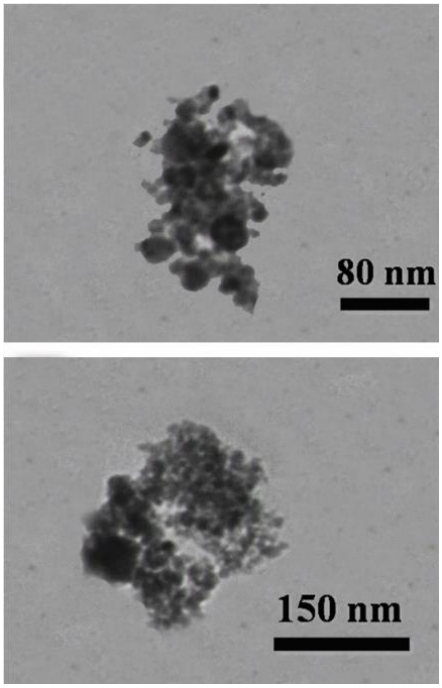

Fig. 6. TEM images of the $Fe_3O_4/Fe_{0.874}Cu_{0.349}W_{0.004}O_{1.525}$ photocatalyst..

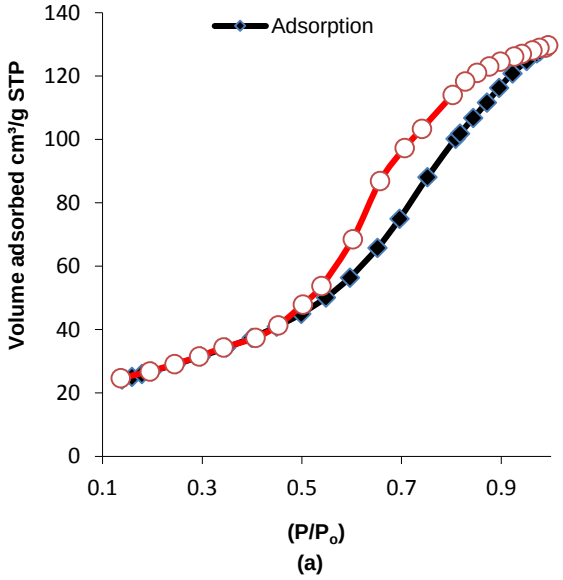

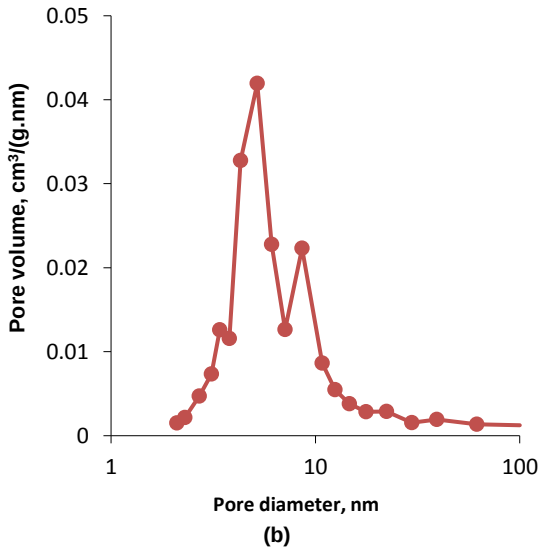

Fig. 7. (a) N_2 adsorption/desorption isotherm, (b) Pore size distribution.

3.4. Effect of pH

Increase in pH increased the negative charge of 2, 4-D; so 2, 4-D photodegradation was increased, and reached its maximum at pH=7. The more increase in pH caused 2, 4-D photodegradation again decreased. In high pH, the 2, 4-D molecules were converted to $C_8H_5(Cl_2)O_3^-$, and the repulsion between negative photocatalyst surface and negatively charged 2, 4-D decreased adsorption and photodegradation processes (Lam et al. 2013; Tang et al. 2015; Mehrabadi and Faghihian. 2019).

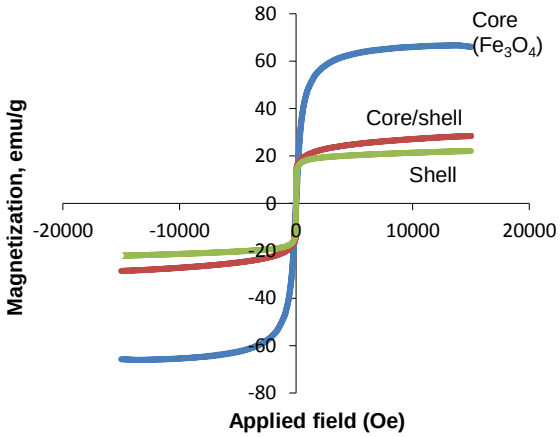

Fig. 8. Magnetic hysteresis curves for core, shell, and core/shell samples.

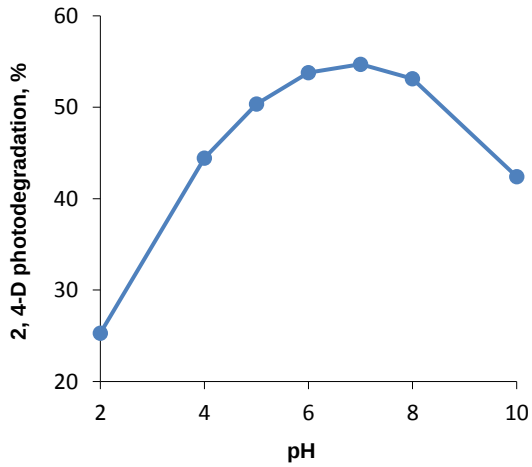

Fig. 9. Effect of pH on 2, 4-D photodegradation; operating conditions: 2,4-D initial concentration 10 mg/L, catalyst dose 1 g/mL, time 120 min.

3.5. Effect of light sources

Fig. 10 shows that ultraviolet light was the most effective on the 2,4 dichlorophenoxyacetic acid (2, 4-D) photodegradation. Sunlight and also light emitting diode (LED) were able to photodegrade 2, 4-D. In the dark condition, 2, 4-D was removed with the maximum yield of 10.7 % which can be attributed to the adsorption process.

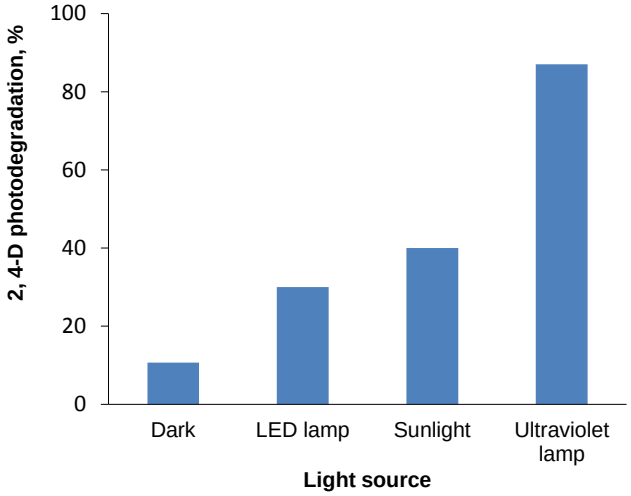

Fig. 10. Effects of different light sources on 2, 4-D photodegradation; operating conditions: 2,4-D initial concentration 10.9 mg/L, catalyst dose 1.4 g/L, pH 8, time 95 min.

3.6. Reaction kinetics

Reaction kinetics is one of the most important factors in the reactor design and determination of the operating conditions. The 2, 4-D photodegradation versus time is shown in Fig. 11. The first order kinetic, Eq. 4 was fitted to the experimental data.

$$\ln\left(\frac{C}{C_0}\right) = -kt \quad (4)$$

where, k was the reaction rate constant in min $^{-1}$, t was time, and C and C_0 were final and initial concentration of 2,4-D; respectively. The R^2 of the fitting was 0.9862 which confirm first order model was corresponded well to the data, and rate constant (k) was 0.0118 min^{-1}.

3.7. Photocatalyst recycling

The reuse of the core/shell magnetic photocatalyst $Fe_3O_4/Fe_{0.874}Cu_{0.349}W_{0.004}O_{1.525}$ was investigated. After each experiment of 2, 4-D photodegradation, the photocatalyst was collected, dried, and reused. As shown in Fig. 12, after fourth cycle of photocatalyst reuse and regeneration, the 2, 4-D photodegradation was nearly constant. A little decrease in the photocatalyst activity can be related to the loss of the photocatalyst in the separation and drying stages.

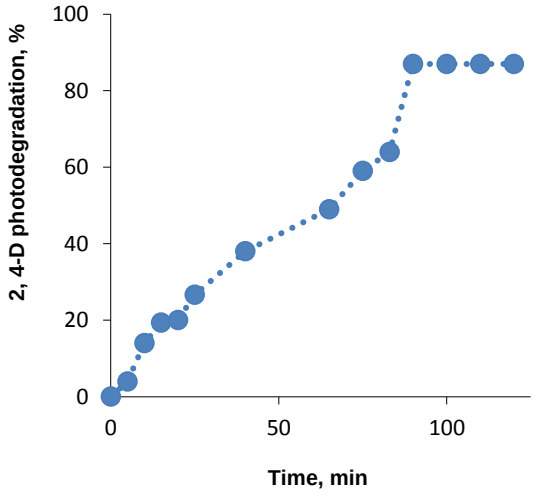

Fig. 11. Effect of time on 2, 4-D photodegradation; operating conditions: 2,4-D initial concentration 10.9 mg/L, catalyst dose 1.4 g/L, pH 8.

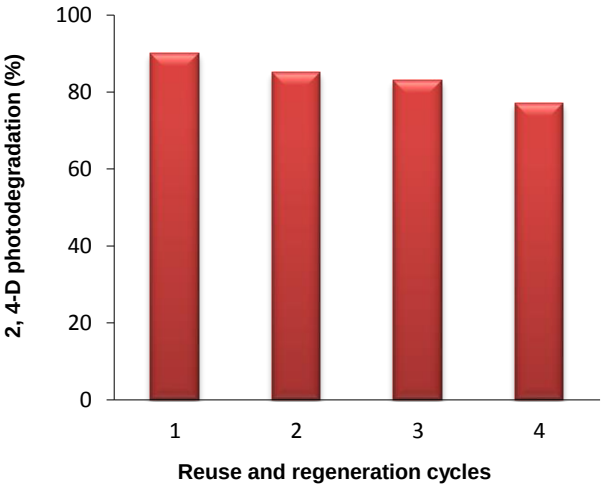

Fig. 12. $Fe_3O_4/Fe_{0.874}Cu_{0.349}W_{0.004}O_{1.525}$ photocatalyst reuse and regeneration cycles; operating conditions: 2,4-D initial concentration 10.9 mg/L, catalyst dose 1.4 g/L, pH 8, time 120 min.

3.8. Comparison with other works

Table 5 compares the results of this work with others. It is clear that the results of $Fe_3O_4/Fe_{0.874}Cu_{0.349}W_{0.004}O_{1.525}$ for 2, 4-D photodegradation are comparable with other works. The $Fe_3O_4/Fe_{0.874}Cu_{0.349}W_{0.004}O_{1.525}$ photocatalyst has the advantage of easy separation from wastewater containing 2, 4-D by an external magnet in addition to high photocatalyst activity.

Table 5. Comparison 2, 4-D photodegradation works.

No.	Photocatalyst	2, 4-D initial concentration, mg/L	Time, min	2, 4-D photodegradation (%)	Reference
1	ZnO/γ-Fe_2O_3	20	240	55.29	Abdulla et al. (2013)
2	Tourmaline-coated TiO_2 Nanoparticles	50	35	90	Bian et al. (2013)
3	MoO_3/ZnO	20	120	100	Lam et al. (2013)
4	Graphene/TiO_2	50	600	95	Huang et al. (2016)
5	Nanorods of Zinc oxide	5	60	96	Meenakshi et al. (2017)
6	Fe_2O_3 doped TiO_2	10	240	48	Razani et al. (2017)
7	Hydrothermally synthesized TiO_2	50	120	96	Sandeep et al. (2018)
8	TiO_2/Chitosan	50	120	92	Balakrishnan et al. (2020)
9	WO_3 doped ZnO	25	120	88.75	Zandsalimi et al. (2020)
10	$Fe_3O_4/Fe_{0.874}Cu_{0.34}W_{0.004}O_{1.575}$	10	90	90	This work

4. Conclusions

The core/shell magnetic photocatalyst, $Fe_3O_4/Fe_xCu_yW_zO_t$, was prepared by co-precipitation method. Box-Behnken method was used to investigate the effects of the $Fe_3O_4/Fe_xCu_yW_zO_t$ constituents on 2, 4-D photodegradation. The results of the experimental model indicated that 2, 4-D photodegradation improved with the increase of Fe solution concentration, but for Cu and W solutions concetrations there were

optimum. The $Fe_3O_4/Fe_{0.874}Cu_{0.349}W_{0.004}O_{1.525}$ was active under irradiation of UV light, LED, and sunlight. The photocatalyst activity was constant after fourth cycle of reuse and regeneration which shows the catalyst reusability. The 2, 4-D photodegradation using $Fe_3O_4/Fe_{0.874}Cu_{0.349}W_{0.004}O_{1.525}$ was comparable with others. These results indicate that $Fe_3O_4/Fe_{0.874}Cu_{0.349}W_{0.004}O_{1.525}$ can be an excellent photocatalyst for photodegradation of poisonous organic materials from water.

Acknowledgements

The authors acknowledge the financial supports of the University of Kurdistan.

References

Abdullah A. H., Mun L.K., Zainal Z., Hussein M.Z., Photodegradation of chlorophenoxyacetic acids by ZnO/γ-Fe_2O_3 nanocatalysts: A comparative study, International Journal of Chemistry 5 (2013) 56-65.

Abdollahi Y., Abdullah A.H., Zainal Z., Yusof N.A., Photodegradation of o-cresol by ZnO under UV irradiation, Journal of American Science 7 (2011) 165-170.

Aghel, S., Bahramifar, N., Younesi, H., Kinetics of photocatalytic degradation of reactive black B using core-shell TiO_2-coated magnetic nanoparticle, $Fe_3O_4@SiO_2@TiO_2$, Journal of Applied Research in Water and Wastewater 6 (2016) 253-259.

Akhlaghian F., Najafi A., $CuO/WO_3/TiO_2$ photocatalyst for degradation of phenol wastewater, Scientia Iranica C 25 (2018) 3345-3353.

Arsalani N., Panahian Y., Nasiri R., Fabrication of novel magnetic F-TiO_2(B)/carbon nanostructures nanocomposites as photocatalysts for malachite green degradation under visible light, Materials Science & Engineering B 251 (2019) 114448.

Atarodi H., and Faghihian H., Selective photodegradation of atrazine by a novel molecularly imprinted nanophotocatalyst prepared on the basis of chitosan, Journal of Photochemistry & Photobiology A 382 (2019) 111892.

Banihashemi M., Dalali N., Sehati N., Farajmand B., Decoration of $Fe_3O_4@SiO_2@ZnO$ as a high performance nanosorbent on a stir bar microextraction device for preconcentration and determination of cadmium in real water samples, Microchemical Journal 154 (2020) 104599.

Balakrishnan A., Appunni S., Gopalram K., Immobilized TiO_2/chitosan beads for photocatalytic degradation of 2,4-dichlorophenoxyacetic acid, International Journal of Biological Macromolecules 161 (2020) 282-291.

Bian X., Chen J., Ji R., Degradation of 2,4-dichlorophenoxyacetic acid (2,4-D) by novel photocatalytic material of tourmaline-coated TiO_2 nanoparticles: kinetic study and model, Materials 6 (2013) 1530-1542.

Browne A.M., Moore P.A., The effects of sublethal levels of 2,4-dichlorophenoxyacetic acid herbicide (2,4-d) on feeding behaviors of the crayfish o. rusticus, Archives of Environmental Contamination and Toxicology 67 (2014) 234-244.

Chang X., Thind S.S., Tian M., Hossain M.M., Chen A., Significant enhancement of the photoelectrochemical activity of nanoporous TiO_2 for environmental applications, Electrochimica Acta 173 (2015) 728-735.

Chenchana A., Nemamcha A., Moumeni H., Doña Rodríguez J.M., Araña J., Navío J.A., González Díaz O., Pulido Melián E., Photodegradation of 2,4-dichlorophenoxyacetic acid over TiO_2(B)/anatase nanobelts and Au-TiO_2(B)/anatase nanobelts, Applied Surface Science 467–468 (2019) 1076-1087.

Chen Z., Lin F., He D., Jiang H., Zhang J., Wang X., Huang M., A hybrid composite catalyst of Fe_3O_4 nanoparticles-based carbon for electrochemical reduction of oxygen, New Journal of Chemistry 41 (2017) 4959-4965.

Costa L.G., Aschner M., Toxicology of pesticides. In: Reference Module in biomedical sciences, Elsevier, pp. 1-9, (2014).

Daneshvar N., Salari D., Khataee A.R., Photocatalytic degradation of azo dye acid red 14 in water on ZnO as an alternative catalyst to TiO_2, Journal of Photochemistry and Photobiology A: Chemistry 162 (2004) 317-322.

Ding J., Liu L., Xue J., Zhou Z., He G., Chen H., Low-temperature preparation of magnetically separable Fe_3O_4@CuO-RGO core-shell heterojunctions for high-performance removal of organic dye under visible light, Journal of Alloys and Compounds 668 (2016) 649-656.

Dong S., Feng J., Fan M., Pi Y., Hu L., Han X., Liu M., Sun J., Sun J., Recent developments in heterogeneous photocatalytic water treatment using visible light responsive photocatalysts: a review, RSC Advances 5 (2015) 14610-14630.

Fiorenza R., Di Mauro A., Cantarella M., Privitera V., Impellizzeri G., Selective photodegradation of 2,4-D pesticide from water by molecularly imprinted TiO_2, Journal of Photochemistry & Photobiology A: Chemistry 380 (2019) 111872.

Gherbi R., Nasrallah N., Amrane A., Maachi R., Trari M., Photocatalytic reduction of Cr(VI) on the new hetero-system $CuAl_2O_4/TiO_2$, Journal of Hazardous Matterials 186 (2011) 1124-1130.

Gu J., Chen H., Jiang F., Wang X., Li L., All-solid-state Z-scheme Co_9S_8/graphitic carbon nitride photocatalysts for simultaneous reduction of Cr(VI) and oxidation of 2,4- dichlorophenoxyacetic acid under simulated solar irradiation, Chemical Engineering Journal 360 (2019) 188-1198.

Habibi-Yangjeh A., Mousavi M., Deposition of $CuWO_4$ nanoparticles over g-C_3N_4/Fe_3O_4 nanocomposite: Novel magnetic photocatalysts with drastically enhanced performance under visible-light, Advanced Powder Technology 29 (2018) 1379-1392.

Hatamzadeh, S., Keramati, N., Mehdipour Ghazi, M., Synthesis and characterization of Ag-ZnO@Clinoptilolite for photocatalytic degradation of Tetracycline, Journal of Applied Research in Water and Wastewater 12 (2019) 138-143.

Hong R.Y., Zhang S.Z., Di G.Q., Li H.Z., Zheng Y., Ding J., Wei D.G., Preparation, characterization and application of Fe_3O_4/ZnO core/shell magnetic nanoparticles, Materials Research Bulletin 43 (2008) 2457-2468.

Hong R.Y., Li J.H., Cao X., Zhang S.Z., Di G.Q., Li H.Z., Wei D.G., On the $Fe_3O_4/Mn_{1-x}Zn_xFe_2O_4$ core/shell magnetic nanoparticles, Journal of Alloys and Compounds 480 (2009) 947-953.

Huang D., Yang T., Mo Z., Guo Q., Quan S., Luo C., Liu L., Preparation of Graphene/TiO_2 Composite Nanomaterials and its photocatalytic performance for the degradation of 2,4-dichlorophenoxyacetic acid, Journal of Nanomaterials 2016 (2016) 5858906.

Huy B.T., Jung D., Phuong N.T.K., Lee Y., Enhanced photodegradation of 2,4-dichlorophenoxyacetic acid using a novel $TiO_2@MgFe_2O_4$ core@shell structure, Chemosphere 184 (2017) 849-856.

Kalambate P.K., Dhanjai, Huang Z., Li Y., Shen Y., Xie M., Huang Y., Srivastava A.K., Core@shell nanomaterials based sensing devices: A review, Trends in Analyyical Chemistry 115 (2019) 147-161.

Khairy M., Polyaniline–$Zn_{0.2}Mn_{0.8}$ Fe_2O_4 ferrite core–shell composite: Preparation, characterization and properties, Journal of Alloys and Compounds 608 (2014) 283-291.

Kundu S., Pala A., Dikshit A.K., UV induced degradation of herbicide 2,4-D: kinetics, mechanism and effect of various conditions on the degradation, Separation and Purification Technology 44 (2005) 121-129.

Lam S.-M., Sin J.-C., Abdullah A.Z., Mohamed A.R., Investigation on visible-light photocatalytic degradation of 2,4-dichlorophenoxyacetic acid in the presence of MoO_3/ZnO nanorod composites, Journal of Molecular Catalysis A: Chemical 370 (2013) 123-131.

Leofanti G., Padovan M., Tozzola G., Venturelli B., Surface area and pore texture of catalysts, Catalysis Today 41 (1998) 207-219.

Macías-Tamez R., Villanueva-Rodríguez M., Ramos-Delgado N.A., Maya-Treviño L., Hernández-Ramírez A., Comparative study of the photocatalytic degradation of the herbicide 2,4-d using WO_3/TiO_2 and Fe_2O_3/TiO_2 as catalysts, Water, Air, and Soil Pollution 228 (2017) 379-390.

Marin-Morales M. A., Ventura-Camargo B.C., Hoshina M.M. Toxicity of Herbicides: Impact on Aquatic and Soil Biota and Human Health. In: Price A., Kelton J., Herbicides: Current research and case studies in use rice, BoD-Books on Demand; pp. 399-443, (2013).

Meenakshi G., Sivasamy A. 2017 Synthesis and characterization of zinc oxide nanorods and its photocatalytic activities towards

degradation of 2,4-D. Ecotoxicology and Environmental Safety 135 (2017) 243-251.

Mehrabadi Z., Faghihian H., Clinoptilolite modified with TiO_2 for simultaneous elimination of two herbicides; 2,4-D and MCPA by UV and sunlight-assisted photocatalytic degradation, Materials Research Bulletin 119 (2019) 110569.

Mirzai M., Akhlaghian F., Rahmani F., Photodegration of ciprofloxacin in water using photocatalyst of zinc oxide nanowires doped with copper and cerium oxides, Water and Environment Journal 34 (2020) 420-431.

Irzapour M., Akhlaghian F., Core/shell magnetic nanoparticles of $Fe_3O_4/Mn_xZn_yFe_{3-x-y}O_4$ for phosphate adsorption from water: effects of adsorbent composition using response surface methodology, Desalination and Water Treatment 137 (2019) 114-124.

Mohite R.G., Garg A., Performance of heterogeneous catalytic wet oxidation for the removal of phenolic compounds: catalyst characterization and effect of pH, temperature, metal leaching and non-oxidative hydrothermal reaction, Journal of Environmental Chemical Engineering 5 (2017) 468-478.

Momeni M.M., Hakimian M., Kazempour A., In-situ manganese doping of TiO_2 nanostructures via single-step electrochemical anodizing of titanium in an electrolyte containing potassium permanganate: A good visible-light photocatalyst, Ceramics International 41 (2015) 13692-13701.

National drinking water regulations: 2,4-D, https://nepis.epa.gov/Exe/ZyPDF.cgi/91022ZI1.PDF?Dockey=91022ZI1.PDF; 1995 (accessed 4 September 2020).

Nasir A.M., Jaafar J., Aziz F., Yusof N., Salleh W.N.W., Ismail, A.F., Aziz, M., A review on floating nanocomposite photocatalyst: Fabrication and applications for wastewater treatment, Journal of Water Process Engineering 36 (2020) 101300.

Pham T.-D., Lee B.-K., Lee C.-H., The advanced removal of benzene from aerosols by photocatalyticoxidation and adsorption of Cu–TiO_2/PU under visible light irradiation, Applied Catalysis B: Environmental 182 (2016) 172-183.

Rabanimehr, F., Farhadian, M., Solaimany Nazar, A.R., Behineh, E.S., Simulation of photocatalytic degradation of methylene blue in planar microreactor with integrated ZnO nanowires, Journal of Applied Research in Water and Wastewater 8 (2021) 36-40.

Razani A, Abdullah A.H., Fitrianto A., Yuosof N.A., Gaya U.I., Sol-gel synthesis of Fe_2O_3-doped TiO_2 for optimized photocatalytic degradation of 2,4- dichlorophenoxy acetic acid, Oriental Journal of Chemistry 33 (2017) 1959-1968.

Rebelo S.L.H., Melo A., Coimbra R., Azenha M.E., Pereira M.M., Burrows H.D., Sarakha M., Photodegradation of atrazine and ametryn with visible light using water soluble porphyrins as sensitizers, Environmental Chemistry Letters 5 (2007) 29-33.

Sandeep S., Nagashree K.L., Maiyalagan T., Keerthiga G., Photocatalytic degradation of 2,4-dichlorophenoxyacetic acid—A comparative study in hydrothermal TiO_2 and commercial TiO_2, Applied Surface Science 449 (2018) 371-379.

Seck E.I., Doña-Rodíguez J.M., Fernández-Rodríguez C., González-Díaz O.M., Araña J., Pérez-Peña, J., Photocatalytical removal of bentazon using commercial and sol–gel synthesized nanocrystalline TiO_2: Operational parameters optimization and toxicity studies, Chemical Engineering Journal 203 (2012) 52-62.

Suresh S., Karthikeyan S., Jayamoorthy K. FTIR and multivariate analysis to study the effect of bulk and nano copper oxide on peanut plant leaves, Journal of Science: Advanced Materials and Devices 1 (2016) 343-350.

Tang L., Zhang S., Zeng G.-M., Zhang Y., Yang G.-D., Chen J., Wang J.-J., Wang J.-J., Zhou Y.-Y., Deng Y.-C., Rapid adsorption of 2,4-dichlorophenoxyacetic acid by iron oxide nanoparticles-doped carboxylic ordered mesoporous carbon, Journal of Colloid and Interface Science 445 (2015) 1-8.

Tang Y., Luo S., Teng Y., Liu C., Xu X., Zhang X., Chen L., Efficient removal of herbicide 2,4-dichlorophenoxyacetic acid from water using Ag/reduced graphene oxide co-decorated TiO_2 nanotube arrays, Journal of Hazardous Materials 241– 242 (2012) 323-330.

Widiyandari H., Purwanto A., Balgis R., Ogi T., Okuyama K., CuO/WO_3 and Pt/WO_3 nanocatalysts for efficient pollutant degradation using visible light irradiation, Chemical Engineering Journal 180 (2012) 323-329.

Wu L., Li A., Gao G., Fei Z., Xu S., Zhang Q., Efficient photodegradation of 2,4-dichlorophenol in aqueous solution catalyzed by polydivinylbenzene-supported zinc phthalocyanine, Journal of Molecular Catalysis A: Chemical 269 (2007) 183-189.

Wu P., Liu Z., Chen D., Zhou M., Wei J., Flake-like NiO/WO_3 p-n heterojunction photocathode for photoelectrochemical water splitting, Applied Surface Science 440 (2018) 1101-1106.

Xie W., Liu L., Cui W., An W., Enhancement of photocatalytic activity under visible light irradiation via the AgI@TCNQ core-shell structure, Materials 12 (2019) 1679.

Youssef A.M., EL-Didamony H., El-Sharabasy S.F., Sobhy M., Hassan A.F., Bluáneke R., Adsorption of 2, 4 dichlorophenoxyacetic acid on different types of activated carbons based date palm pits: kinetic and thermodynamic studies, International Research Journal of Pure & Applied Chemistry 14 (2017) 1-15.

Yusa V., Millet M., Coscolla C., Roca M., Analytical methods for human biomonitoring of pesticides. A review, Analytica Chimica Acta 891 (2015) 15-31.

Zandsalimi Y., Maleki A., Shahmoradi B., Dehestani S., Rezaee R., McKay G., Photocatalytic removal of 2,4-Dichlorophenoxyacetic acid from aqueous solution using tungsten oxide doped zinc oxide nanoparticles immobilised on glass beads, Environmental Technology (2020).